

Prediction of the blade trailing-edge noise of an axial flow fan

Alain GUEDEL
CETIAT
Villeurbanne, France

Mirela ROBITU
CETIAT
Villeurbanne, France

Nicolas DESCHARMES
CETIAT
Villeurbanne, France

Didier AMOR
Fläkt Solyvent-Ventec
Mezzieu, France

Jérôme GUILLARD
Fläkt Solyvent-Ventec
Mezzieu, France

ABSTRACT

The objective of this work is to predict the trailing-edge noise of axial fans with an analytical model deduced from an extension of Amiet's formulation. The input data of the acoustic model are the frequency spectra and the spanwise correlation length scales of the wall-pressure fluctuations on the blade suction side close to the trailing edge.

This model was successfully validated in former studies on single steady airfoils in anechoic wind tunnels and, to a lesser extent, on an axial fan equipped with small unsteady pressure transducers flush mounted on the blade suction side. The present research is carried out on a 6-blade axial fan no longer equipped with embedded pressure transducers. The input data of the prediction are then deduced from non-dimensional spectra and correlation lengths of the pressure fluctuations measured in the previous study and RANS simulations performed on the test fan. A validation of the prediction method is made by comparing the predicted and measured sound power spectra of the fan for two blade pitch angles and different operating points.

INTRODUCTION

Broadband noise is very often the major part of the noise radiated by domestic and industrial fans. For low-speed fans the contribution of the broadband noise to the overall A-weighted sound power level is indeed often much higher than the contribution of the tonal noise at harmonics of the blade passage frequency. The main broadband noise sources of axial-flow fans are due to: interaction of blades with inflow

turbulence, vortex shedding noise, tip vortex noise, rotating stall, and blade trailing edge noise.

The first mechanism provides a major contribution when the inlet flow turbulence is significant, typically when the turbulence intensity is higher than 2 to 2.5%, which is the case for instance on an axial fan behind a heat exchanger. This source should be almost negligible when the fan operates in a non-disturbed flow field such as that at the entrance of a free-inlet axial fan with a well-designed bellmouth and a fan drive either far upstream or downstream from the impeller.

Vortex shedding noise, associated with von Karman vortices in the blade wake, occurs when the thickness of the blade trailing edge is larger than the boundary layer thickness. A sharp trailing edge is therefore beneficial to suppress this mechanism. Furthermore, the signature of vortex shedding noise on the fan spectrum is not noticeable, even with a blunt trailing edge, if the vortex-shedding frequency lies within the frequency range of the boundary layer disturbances.

Tip vortex noise is due to the interaction of the flow in the tip clearance with the blade. The amplitude of this source usually decreases when the tip clearance is reduced but the actual noise mechanism is not well understood yet due to the complex flow pattern in the blade tip area.

Rotating stall, which occurs at reduced flow rates and induces aerodynamic flow instabilities, substantially increases the amount of noise at low frequency.

Blade-trailing edge noise occurs when the turbulent boundary layer on the blade suction side is convected past the trailing edge, a part of the turbulent energy being converted into acoustic energy that radiates to the far-field. This source,

which prevails over the other sources when the inlet flow turbulence is low, corresponds to the minimum noise level radiated by a fan. For this reason this paper is focused on trailing-edge noise in order to find blade geometry that could reduce this noise in the end. This mechanism as well as turbulence-interaction noise has extensively been studied on stationary airfoils in wind tunnels in order to validate prediction models [1] to [3].

The objective of this paper is to present a prediction method of the blade trailing-edge noise of a low-pressure axial fan based on an extension of Amiet's formulation on isolated airfoil, due to Roger and Moreau [4]. The model was experimentally validated first on fixed airfoils in wind tunnels [5], [6] then, to a lesser extent, on rotating blades [7], [8], [9], [10]. This analytical model, which uses the frequency spectra and spanwise correlation length scales of the wall-pressure fluctuations on the blades as input data, is succinctly described in the next section with comparisons between experiment and prediction on a four-blade axial fan equipped with flush-mounted microphones on the suction side near the trailing edge.

Several alternative models to that of Amiet are proposed for the trailing edge noise prediction, which are detailed for instance in [11].

The next stage, which is the core of this paper, consists in the prediction of the trailing-edge noise spectrum of a six-blade axial fan not equipped with pressure transducers from a semi-empirical approach. The idea is to deduce the input data of the prediction model from non-dimensional spectra and correlation lengths of the blade pressure fluctuations, measured on the four-blade fan in the previous study, and RANS flow simulations on the six-blade fan. This approach is based on the assumption that these generic non-dimensional data are representative of the statistics of the blade fluctuating pressure field on a variety of axial fans of similar geometry. If it is proved to be validated with reasonable accuracy on the present fan it may be expected to be valid for the prediction of the trailing-edge noise of other axial fans of the same type.

A complete CFD simulation to obtain the input data of the acoustic prediction directly is indeed totally unrealizable with the numerical tools currently available [6].

CFD calculations and comparisons of measured and predicted sound power spectra on the six-blade fan are presented with a discussion on the validity of this semi-empirical prediction.

TRAILING-EDGE NOISE MODEL

Stationary airfoil

The trailing-edge noise prediction is made with an extension of Amiet's analytical formulation for an isolated airfoil. This extension proposed by Roger and Moreau [4] accounts for the effects of a finite chord length and far-field radiation away from the mid-span plane. According to [8], for low rotation Mach numbers, the far-field sound pressure spectrum radiated in the mid-span plane by a fixed airfoil in a uniform flow field reads:

$$S_{pp}(\bar{x}, \omega) = \left(\frac{kc \sin \theta}{2\pi R} \right)^2 \frac{L}{2} \left| L' \left(x_1, \frac{\omega}{U_0}, 0 \right) \right|^2 \Phi_{pp}(\omega) l_y(\omega) \quad (1)$$

with:

S_{pp} : sound pressure spectrum (dB/Hz)

R: distance between the mid-span trailing edge and the observer (m)

x_1 : coordinate of the observer along the airfoil chord

θ : angle between the chordwise and the observer directions ($\theta = 0^\circ$ in the downstream direction)

c: airfoil chord length (m)

L: airfoil span (m)

$|L'|$: aeroacoustic transfer function

Φ_{pp} : spectrum of the wall-pressure fluctuations (dB/Hz)

l_y : spanwise correlation length scale of the wall-pressure fluctuations (m)

ω : angular frequency (rad/s)

k: acoustic wavenumber (-)

U_0 : velocity of the uniform flow (m/s).

Equation (1) applies to a non-compact airfoil with large aspect ratio ($L/c > 1$). The equation is slightly more complicated for an airfoil of small aspect ratio and when the observer is away from the airfoil mid-span [4]. Furthermore, Amiet's formulation strictly applies to slightly loaded airfoils with small camber, thickness and angle of attack.

The statistics of the turbulent wall-pressure fluctuations, namely the frequency spectrum and the spanwise correlation length scale, are the input data of the model. These quantities have to be assessed slightly upstream of the trailing edge for reasons detailed in [2]. In practice, for airfoils in incidence and rotating blades the pressure fluctuations near the trailing edge are of much larger amplitude on the suction side than on the pressure side, so that Φ_{pp} and l_y have to be determined on the suction side only.

The aeroacoustic transfer function L' between the turbulent wall-pressure fluctuations and the far-field sound pressure fluctuations is determined analytically on the basis of purely acoustic arguments. Its expression, given in [4], [8] is a function of chord length, c, mean flow velocity, U_0 , convection velocity of the wall-pressure field near the trailing edge, U_c , and frequency, f.

Very good agreements have been obtained between predicted and measured far-field sound pressure spectra for a flat plate [8] as well as for single airfoils of various shapes at different angles of attack in anechoic wind tunnel [3]. In all these cases the input data Φ_{pp} and l_y were obtained from measurement with flush-mounted microphones on the airfoils.

Rotating blade

Similar to the approach implemented in [7] for the prediction of the trailing-edge noise of an helicopter rotor, the stationary airfoil model may be extended to a rotating blade with the following adjustment : the blade is split into several segments along its span¹ and the airfoil theory is applied to each segment, assuming that the circular motion is locally equivalent to a translational motion. This assumption is reliable if the trailing-edge noise frequencies are much higher than the rotational frequency. The far-field sound radiation from a given rotating segment is obtained by averaging the sound pressure spectra radiated by the blade segment at several circumferential locations, applying a Doppler factor to account for the relative motion of the source with respect to the observer. The flow velocity is assumed parallel to the chord line according to the weakly loaded airfoil assumption. As stated in [12], the transposition formula is written as:

$$S_{pp}(\bar{x}, \omega) = \frac{B}{2\pi} \int_0^{2\pi} \frac{\omega_c(\Psi)}{\omega} S_{pp}^\Psi(\bar{x}, \omega_c) d\Psi \quad (2)$$

Where $S_{pp}^\Psi(\bar{x}, \omega_c)$ is the sound pressure spectrum that is radiated from the current blade segment at angle Ψ ignoring the Doppler frequency shift, and $\frac{\omega_c(\Psi)}{\omega} = 1 + M \sin \theta \sin \Psi = 1 - M_r$ where (θ, Ψ) are the radiation angle to the axis and the circumferential angle, respectively.

Furthermore, as Amiet's model applies to isolated airfoils this approach is valid for low solidity impellers (chord length noticeably smaller than blade spacing).

Comparison of prediction and experiment on a four-blade axial fan fitted with pressure transducers

The test fan (Fig. 1(a)) is an axial fan of 800-mm diameter made up of four blades in plastic with the following characteristics:

- tip radius: 400 mm
- hub/tip ratio: 0.34
- chord length: 135 mm (nearly constant along the span)
- maximum thickness: 4 mm
- blade pitch angle β_0 : adjustable from 15 to 35° (blade tip angle counted from the rotation plane)
- average tip clearance: 5 mm
- rotation speed: 600 rpm.

To obtain the input data of the model two of the blades are fitted with a set of six small flush-mounted microphones at two radial positions (at mid-span and close to the blade tip). These

¹ A division of the blade into 6 segments is a good compromise as found in a preliminary study. This number of segments was kept constant in all the predictions.

pressure transducers, manufactured by Knowles Acoustics, have a diameter and a length of 2.5 mm. They are embedded in the blades according to the set-up shown in Fig. 1 (b). Four transducers are on the same spanwise line at 10 mm from the trailing edge to get the average spectra and correlation length scales of the pressure fluctuations. The two others are 5 mm chordwisely spaced from the formers to deduce the convection speed of the turbulent fluctuations that is used in the aeroacoustic transfer function in equation (1). More details on the insertion of the pressure sensors in the blades are given in [12]. The signals of the microphones are transmitted to the spectrum analyzer via a 14-channel slip ring.

The fan is unducted at its inlet and outlet (category A installation according to ISO fan standards). A layout of the whole test facility is shown in Fig. 2. The fan is installed on a concrete partition between two reverberant rooms of quite different sizes, the bigger room being on the inlet side. The auxiliary fan driven by an inverter allows to adjust the operating point of the test fan. The flowrate and the pressure of the test fan are measured according to standard ISO 5801. The fan sound power levels in one-third octave band are measured in both reverberant rooms according to ISO 13347-2 to obtain the overall "inlet + outlet" sound power levels of the fan for each operating point, which are compared to the prediction.

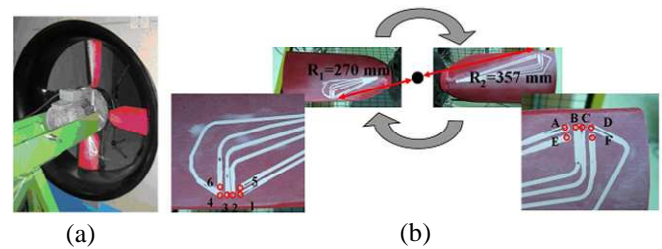


Fig. 1 (a): Test fan; (b): Details of the pressure transducers on the blades

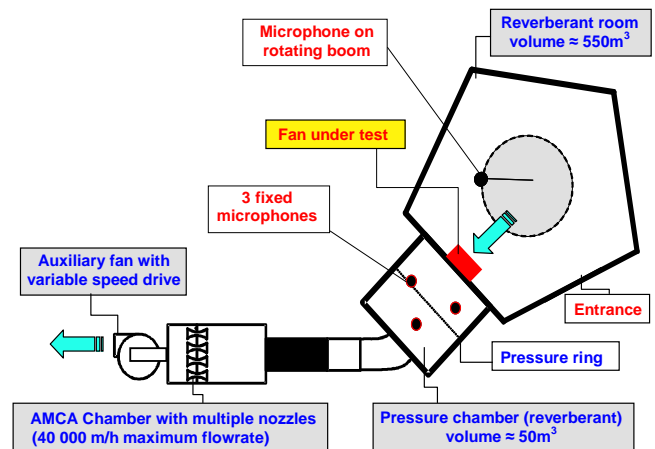


Fig. 2 Test facility layout

Fig. 3 shows a comparison of the measured and predicted one-third octave sound power spectra of the four-blade impeller for a blade angle $\beta_0 = 30^\circ$ at free delivery point (maximum flowrate $Q_{v,max}$ i.e. zero fan static pressure). Except in a frequency range between 315 and 1000 Hz where the two

spectra merge, the prediction is significantly lower than the experiment.

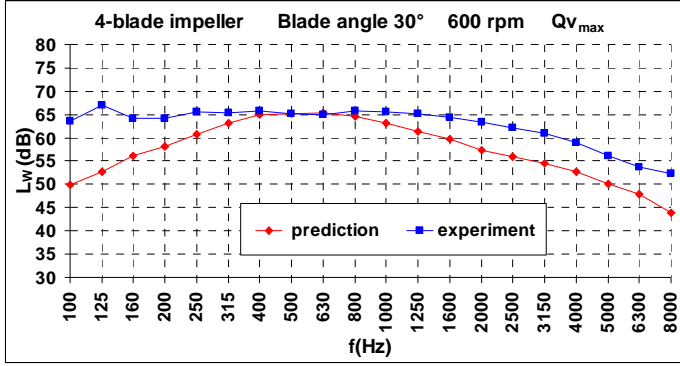


Fig. 3 Comparison of predicted and measured one-third octave "inlet + outlet" sound power levels $\beta_0 = 30^\circ$, $Q v_{max}$

For the same blade angle $\beta_0 = 30^\circ$ the difference in levels $\Delta L_W(f)$ between the measured and predicted spectra is plotted in Fig. 4 for several flowrates between $0.63 Q_{v_{max}}$ and $Q_{v_{max}}$. The curves of the figure have similar shapes and ΔL_W is always positive, which means that the prediction always underestimates the sound level whatever the frequency and the operating point. Several reasons may explain the discrepancies between prediction and experiment, which are developed later on in the paper.

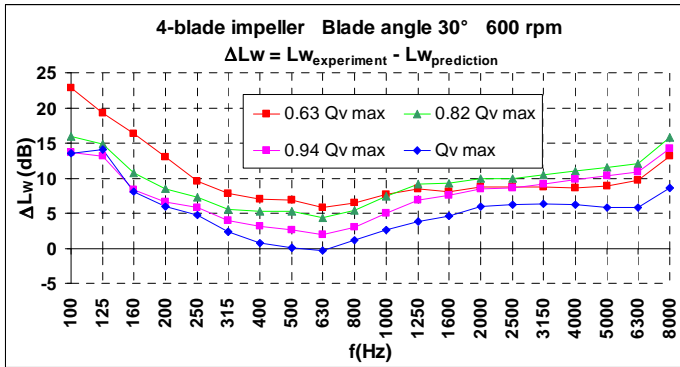


Fig. 4 Difference in levels ΔL_W between measured and predicted sound power spectra at various operating points, $\beta_0 = 30^\circ$

IMPLEMENTATION OF THE MODEL ON A SIX-BLADE AXIAL FAN

Non-dimensional input data of the model

The input data of the prediction are the spectra and spanwise correlation length scales of the wall-pressure fluctuations on the blade suction side close to the trailing edge. As already mentioned these data have been measured with flush-mounted microphones at two radial locations on the four-blade impeller described above. Examples of measured

turbulent pressure spectra are presented in Fig. 5 in non-dimensional coordinates defined by:

$$St = \frac{2\pi f \delta^*}{U_e} \quad (3)$$

$$\tilde{\Phi}_{pp} = \frac{\Phi_{pp}(f)}{\pi \rho_0^2 \delta^{*2} U_e^3} \quad (4)$$

where the so-called outer variables δ^* and U_e are the displacement thickness and external flow velocity of the blade boundary layer over the pressure transducers. These parameters have been obtained from RANS simulations similar to those presented later on in the paper.

$\Phi_{pp}(f)$ is a wall-pressure spectrum (dB ref. $1 \text{ Pa}^2/\text{Hz}$)

averaged over the spectra of the pressure transducers situated in the same spanwise area.

f: frequency (Hz)

ρ_0 : air density (kg/m^3)

The spectra in Fig. 5, which have been obtained for two blade angles $\beta_0 = 20^\circ$ and 30° , two spanwise locations of the pressure transducers and different operating points, show some dispersion especially at high frequency.

The spectrum averaged over all the spectra of Fig. 5 is compared in Fig. 6 to non-dimensional wall-pressure spectra measured on single airfoils in wind tunnel and some rotating blades of impellers. This average spectrum (shown in red in Fig. 6) passes through the middle of the other spectra except at low frequency ($St < 0.3$) where it is above.

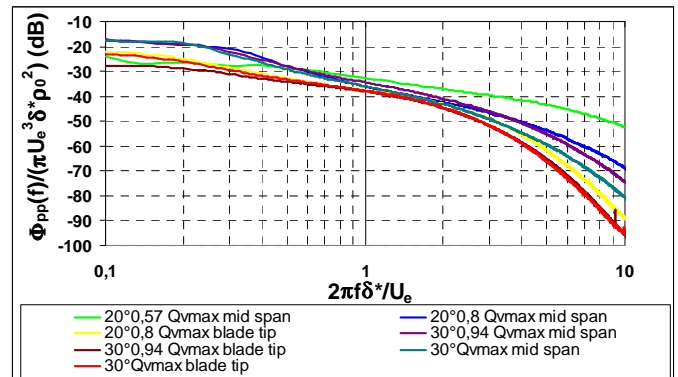


Fig. 5 Non-dimensional wall pressure narrowband spectra of the four-blade impeller at two blade angles $\beta_0 = 20^\circ$ and 30° and various operating points

The spanwise correlation lengths $l_y(f)$ of the four-blade impeller have been measured according to the method described in [12] for $\beta_0 = 20^\circ$ and 30° and different operating points. The average non-dimensional correlation length l_y / δ^* for this fan is compared in Fig. 7 to other correlation lengths measured on different fixed airfoils in wind tunnel. The average curve in red passes through the other curves.

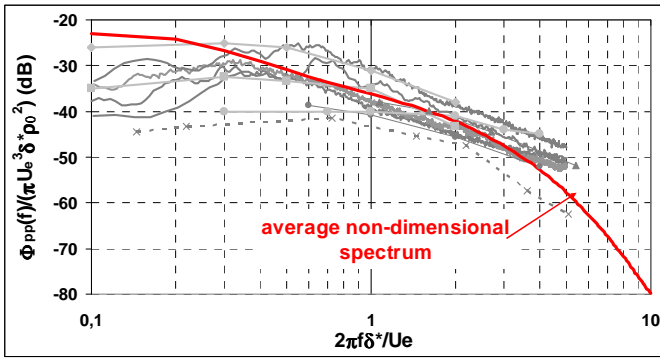


Fig. 6 Comparison of the average non-dimensional wall-pressure spectrum of the 4-blade fan with other measured spectra

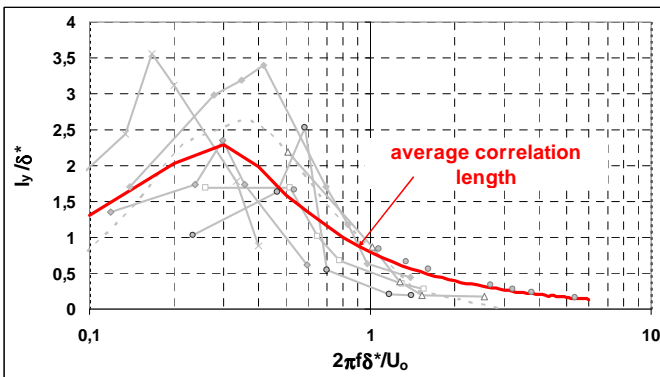


Fig. 7 Comparison of the average non-dimensional correlation length scales of the wall-pressure fluctuations of the 4-blade fan with other test data

The curves represented with red lines in Fig. 6 and Fig. 7 will be used in the prediction.

Experimental set-up

Fan geometry. The test fan is an industrial axial flow fan with six aerofoil blades made up of die-cast aluminium alloy (Fig. 8). The motor is on the inlet side (Fig. 8 (a)). The support arms of the motor, which hold the casing, are far enough from the blades to minimize the turbulence of the flow entering the impeller.

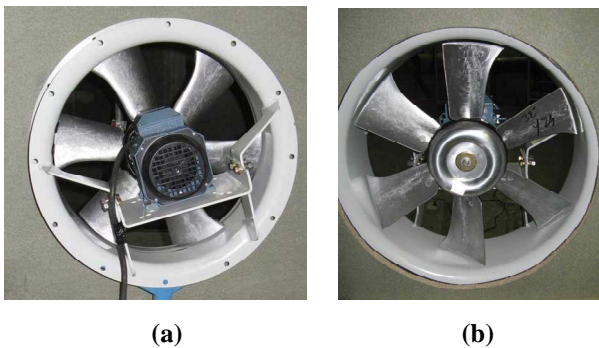


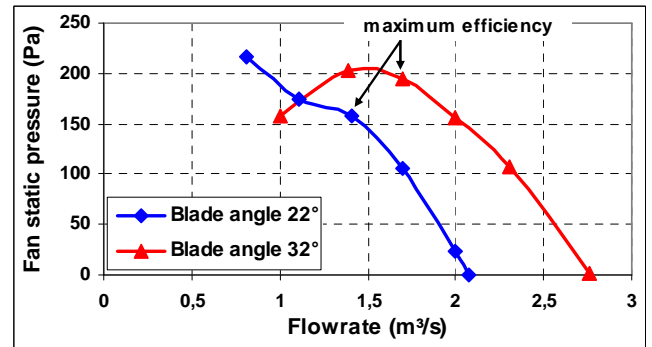
Fig. 8 Views of the 6-blade test fan (a) Inlet; (b) Outlet

The main characteristics of this impeller are:

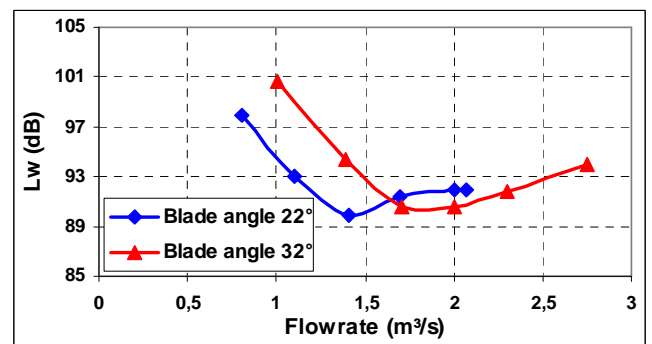
- impeller diameter: 490 mm
- hub/tip ratio: 0.33
- chord length: 83 mm at the hub and 139 mm at the tip
- tip maximum blade thickness: 3 mm
- blade pitch angle adjustable
- average tip clearance: 4.5 mm
- rotation speed: 1450 rpm.

Fan performance and sound levels. The aerodynamic and acoustic performances of the fan have been measured according to ISO standards in the test facility shown in Fig. 2 for two blade angles $\beta_0 = 22^\circ$ and 32° (blade tip angle counted from the rotation plane).

Fig. 9(a) shows the fan performance curves (static pressure versus volume flow) and Fig. 9 (b) the overall fan "inlet + outlet" sound power levels for the two blade angles. The best efficiency points (BEP), shown in Fig. 9(a), occur at $0.68 Q_{V_{max}}$ for $\beta_0 = 22^\circ$ and $0.62 Q_{V_{max}}$ for $\beta_0 = 32^\circ$. For both angles the sound level reaches a minimum at the BEP and strongly increases at low flow rate according to the usual trend observed on axial fans.



(a)



(b)

Fig. 9 Measured fan curves $\beta_0 = 22^\circ$ and 32° (a) Fan static pressure (Pa); (b) Overall sound power levels (dB)

Basis of the prediction method

Unlike the four-blade impeller the blades of the six-blade fan are no more equipped with pressure transducers. The prediction process includes different steps summarized in Fig.

10. The noise model requires dimensional spectra and spanwise correlation lengths of the wall-pressure fluctuations on the blade suction side of the fan under consideration. These input data are deduced from non-dimensional spectrum and correlation length, like those shown above, and blade boundary layer parameters δ^* and U_e obtained by CFD simulations for each blade angle and operating point.

The output of the model is a far-field sound pressure spectrum at a distance R and an observation angle θ from the impeller axis. The predicted one-third octave sound power spectrum is deduced from the sound pressure spectra calculated in a horizontal plane on a circle of radius R surrounding the fan at several angles θ . The choice of relevant values for θ is made according to ISO 13347-3. Due to axisymmetry conditions six sound pressure spectra calculated on half a circle are enough to obtain the sound power spectrum radiated by the fan inlet and outlet.

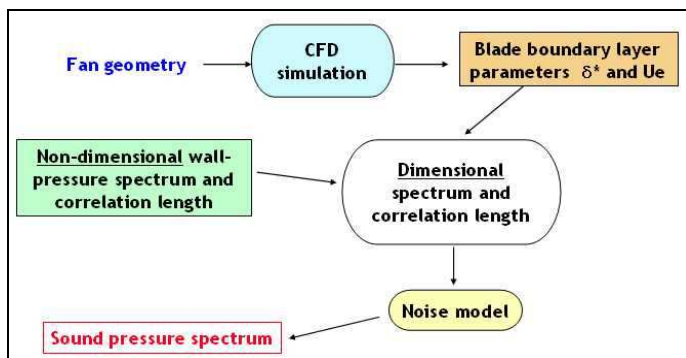


Fig. 10 Prediction method

CFD simulations and post-processing on the six-blade fan are presented below. Results of the acoustic prediction are compared with measured data in a following paragraph.

CFD simulations and post-processing

A three-dimensional CFD modeling of the fan mounted in the test facility is conducted in order to obtain the characteristics of the boundary layer, i.e. the displacement thickness, δ^* , and the external velocity, U_e , of the boundary layer. The simulations are carried out under steady state conditions.

Firstly, the cleaning up of the CAD geometry provided by the fan manufacturer and the surface meshing of calculation domain are carried out in ANSA pre-processing tool. The surface mesh is generated with progressive element size. Then, because of the complexity of the blade geometry, an unstructured tetrahedral volume mesh is generated using TGrid. A refined mesh is realized close to the fan in order to capture the flow variation (large velocity or pressure gradient) due to the presence of the solid elements. The mesh has been done in order to obtain a reasonable compromise between better accuracy and shorter computational time. The final mesh grid of the calculation domain is an unstructured grid of 1,650,000 elements.

The fan test facility is modeled with multiple reference frame approach (MRF). The fluid zone in the fan area is modeled as a rotating reference frame. Fluid surrounding fan area is modeled in a stationary frame.

The Navier–Stokes equations with $k-\epsilon$ realizable turbulence model including enhanced wall treatment are used. To simulate this model a first order upwind scheme is used first, then once the solution is converged a second order upwind differencing scheme is used. To check problem of convergence, in addition to the default residuals a surface monitor is set at the inlet MRF region to monitor the mass flow rate. The convergence of the mass flow rate provides an indication of the physical solution convergence.

Computational grid and boundary conditions. The computation domain and the boundary conditions are illustrated in Fig. 11. The computation domain is divided into two regions. The first region corresponds to the main flow outside the fan, a stationary region that consists of 635,677 elements. The second region (MRF region), which corresponds to the fluid near the fan, consists of 983,381 elements. The MRF region includes rotating parts (blade, hub) and stationary parts (motor that is circumferentially symmetric).

The Inlet is defined as a “Mass Flow Inlet”. The Outlet is defined as a “Pressure Outlet” with static pressure equal to zero. The fan walls are modeled as rotational moving walls with zero velocity relative to the adjacent cell zone. The other walls of the domain are modeled as stationary walls. To reduce the problem size, the flow field is simulated for a single blade passage by using periodic boundary conditions, the calculation domain corresponds to 1/6 of the total domain. In order to obtain the fan performance curve simulations were made for different inlet mass flow rates. The fluid zone in the fan area is rotating at 1450 rpm. The simulations take approximately 50 hours per case with a single processor.

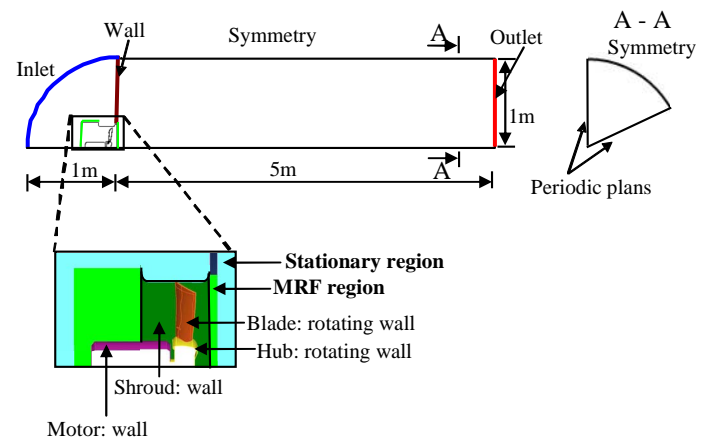


Fig. 11 Dimensions and boundary conditions of the calculation domain.

Results.

Fig. 12 shows examples of results deduced from the RANS simulations. A cartography of the relative total pressure in the mid-span section is presented in Fig. 12 (a) for $\beta_0 = 32^\circ$

and a flowrate of $2\text{ m}^3/\text{s}$ ($0.72 Q_{v_{\max}}$). The boundary layer on the blade suction side is clearly visible. The black straight line reproduces the normal to the blade surface along which the velocity profile is extracted from the calculation.

Fig. 12 (b) and (c) show for $\beta_0 = 22^\circ$ and 32° respectively the tip vortex which separates from the blade in the first half part of the chord.

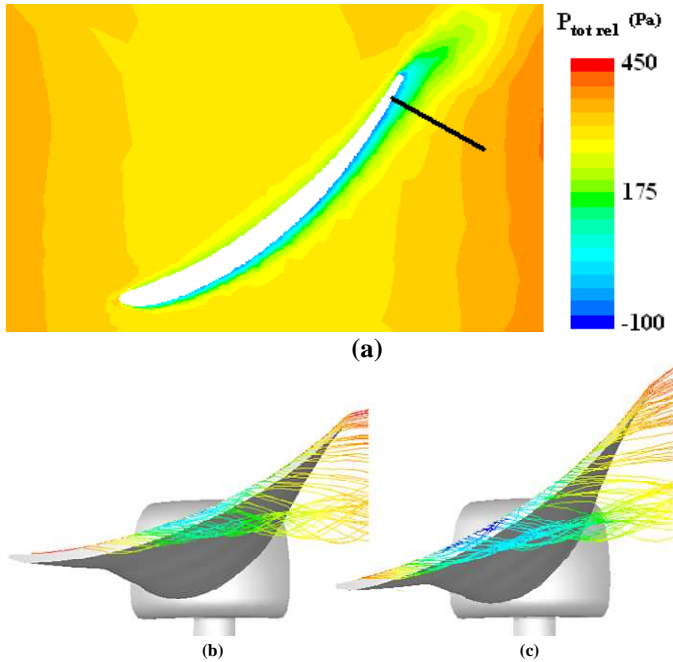
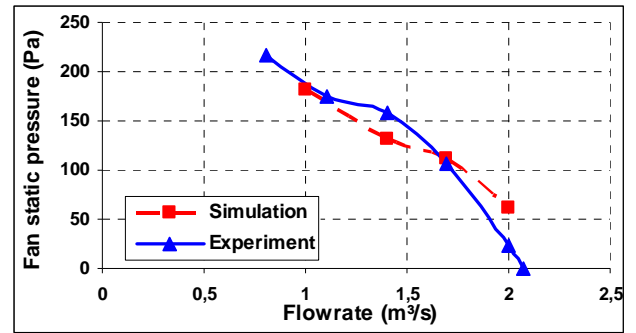
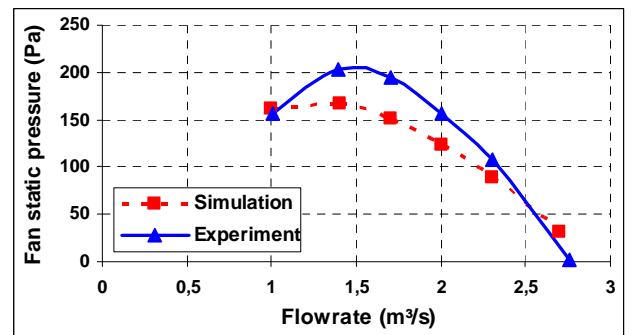


Fig. 12 Examples of RANS simulation results (a) Relative total pressure in the mid-span section $\beta_0 = 32^\circ$; Path lines on the blade tip (b) $\beta_0 = 22^\circ$, $Q_v = 0.68 Q_{v_{\max}}$; (c) $\beta_0 = 32^\circ$, $Q_v = 0.62 Q_{v_{\max}}$.

The fan curves obtained numerically are compared with the test results in Fig. 13. The simulation is close to the experiment for $\beta_0 = 22^\circ$, but it underestimates the static pressure at low flowrate for $\beta_0 = 32^\circ$ in a portion of the curve where the flow is unstable due to rotating stall.



(a)



(b)

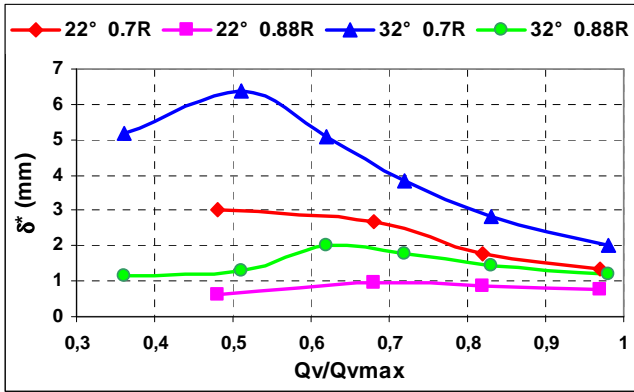
Fig. 13 Comparison of the measured and simulated fan performance curves (a) $\beta_0 = 22^\circ$; (b) $\beta_0 = 32^\circ$

Fig. 14 show the evolution of the calculated displacement thickness, δ^* , and external velocity, U_e , with flowrate for $\beta_0 = 22^\circ$ and 32° and the two spanwise locations of interest $r = 0.7 R$ and $0.88 R$. As seen in Fig. 14 (a) when the flow decreases from $Q_{v_{\max}}$, δ^* increases, reaches a maximum, then decreases when $Q_v/Q_{v_{\max}} < 0.5$ to 0.6 . In Fig. 14 (b), U_e decreases almost linearly with flow when $Q_v/Q_{v_{\max}} \geq 0.65$, then it decreases more rapidly for lower flowrate at $r = 0.88 R$.

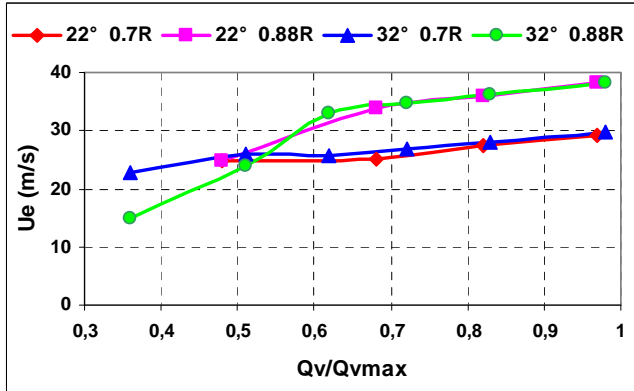
VALIDATION OF THE MODEL

Comparison of predicted and measured fan sound power spectra

Fig. 15 and Fig. 16 show the measured and predicted one-third octave sound power spectra between 100 Hz and 8 kHz for the same flowrates at $\beta_0 = 22^\circ$.



(a)



(b)

Fig. 14 Evolution of the parameters of the blade boundary layers with flowrate at two spanwise locations 0.7 R and 0.88 R $\beta_0 = 22^\circ$ and 32° (a) δ^* ; (b) U_e

Significant differences are observed between the two sets of spectra:

- the predicted levels considerably fall down at low frequency (below about 400 Hz) while the measured levels remain almost constant between 100 and 1000 Hz
- the scattering between the spectra above 1 kHz is much higher on the prediction than on the experiment.

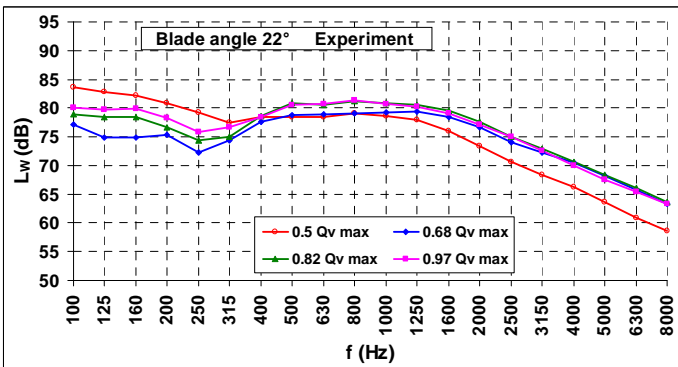


Fig. 15 Measured one-third octave sound power spectra at various operating points $\beta_0 = 22^\circ$

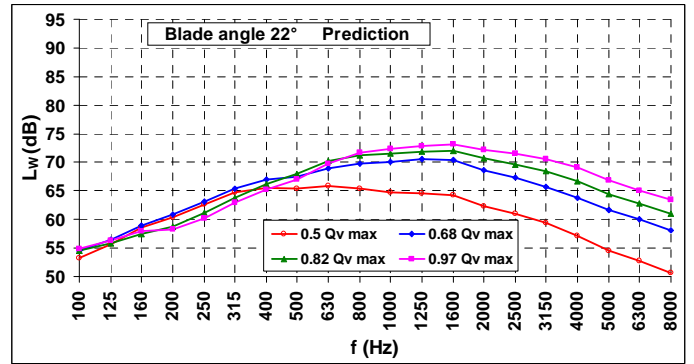
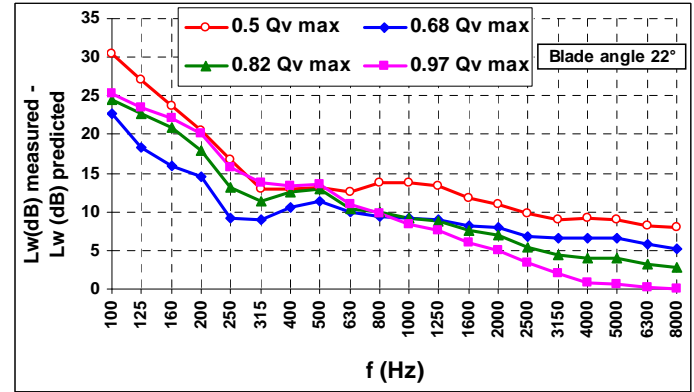
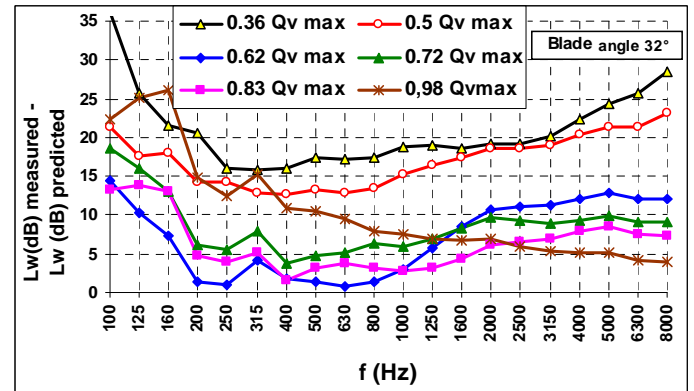


Fig. 16 Predicted one-third octave sound power spectra at various operating points $\beta_0 = 22^\circ$



(a)



(b)

Fig. 17 Difference in levels between measured and predicted sound power spectra (a) $\beta_0 = 22^\circ$; (b) $\beta_0 = 32^\circ$

Fig. 17 shows the difference in levels between measured and predicted sound power spectra $\Delta L_w(f)$ for both angles $\beta_0 = 22^\circ$ and 32° and different operating points. The prediction underestimates the sound levels in a way that depends on frequency and flowrate. The difference $\Delta L_w(f)$ is very high for $\beta_0 = 32^\circ$ when $Q_v \leq 0.5 Q_{vmax}$.

Improvements in the prediction

Several reasons may explain the large discrepancies observed between the measured and predicted spectra, in particular:

- the inaccuracy of the input data of the acoustic model
- the contribution of other noise sources than trailing-edge noise to the fan sound levels.

The inaccuracy of the input data has been assessed by investigating the influence of the non-dimensional wall-pressure spectrum and the blade boundary layer parameters, δ^* and U_e , on $\Delta L_W(f)$.

The contribution of tip clearance noise and secondary flow near the hub at low flowrate conditions, which are not included in the prediction model, is a very likely additional source that could partly explain the systematic underestimation of the prediction. The interaction noise of the blades with inlet turbulence is very unlikely since the amplitude of this source should increase with flow velocity. This is not what is actually observed here since all the results obtained in this study show that the prediction is closer to the experiment at high flow conditions.

Influence of the non-dimensional wall-pressure spectrum. In order to assess the influence of the wall-pressure spectrum on the prediction Fig. 18 shows three examples of non-dimensional wall-pressure spectra obtained with the four-blade impeller. Spectrum 1 is the average narrowband spectrum already shown in red in Fig. 6, which is used in the prediction above. Spectra 2 and 3 have already been presented with the same colors in Fig. 5. They have been chosen according to the following arbitrary criterion: spectrum 2 has the highest level of all the spectra in Fig. 5 for $St < 0.4$ whilst spectrum 3 has the highest level when $St > 1$. $\Delta L_W(f)$ is plotted with these three spectra as input data in Fig. 19 for $\beta_0 = 32^\circ$ and $Q_v = 0.72 Q_{vmax}$.

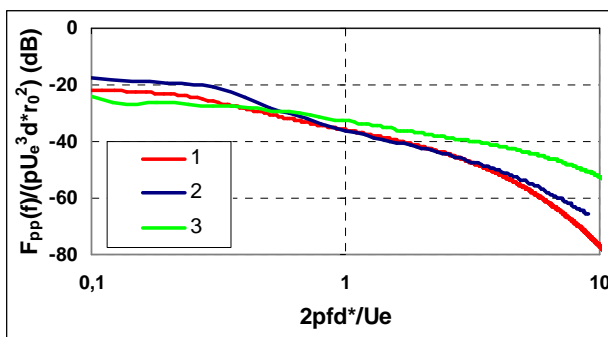


Fig. 18 Examples of non-dimensional narrowband wall-pressure spectra (dB/Hz)

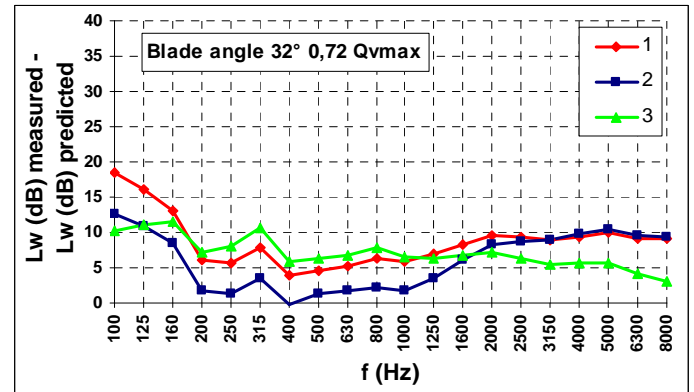


Fig. 19 Difference in levels between measured and predicted sound power spectra with the non-dimensional wall-pressure spectra of Fig. 18, $Q_v = 0.72 Q_{vmax}$, $\beta_0 = 32^\circ$

A significant reduction of $\Delta L_W(f)$ is observed between 200 Hz and 1000 Hz with spectrum 2 in comparison with the two other spectra. Conversely, $\Delta L_W(f)$ is lower with spectrum 3 when $f > 2$ kHz.

Influence of δ^* and U_e . Since $\Delta L_W(f)$ is systematically higher at low flowrate it may be possible that the CFD calculations underestimate the values of δ^* and U_e in a flow range close to rotating stall where the flow is unsteady. An extrapolation of δ^* and U_e has been made according to the dotted lines shown in Fig. 20 and Fig. 21. The influence of the modifications of δ^* and U_e on $\Delta L_W(f)$ is seen in Fig. 22, which shows results obtained for $\beta_0 = 32^\circ$ and two flowrates, with the previous and modified values of these parameters. The extrapolated values clearly reduce the gap between prediction and experiment, which could confirm that the initial values were underestimated. This assumption was recently reinforced by the result of a new RANS simulation with a $k-\omega$ SST instead of a $k-\epsilon$ realizable model, which shows values of δ^* and U_e that are quite close to the extrapolated values of Fig. 20 and Fig. 21 at low flowrate.

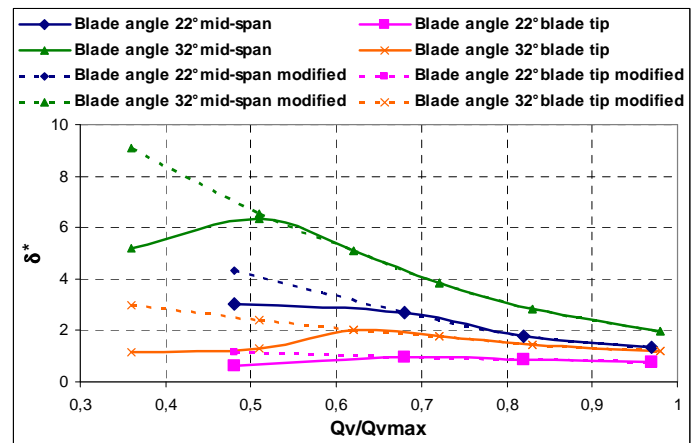


Fig. 20 Evolution of δ^* with flowrate (the dotted lines are obtained from an extrapolation of the calculated data at high flowrate)

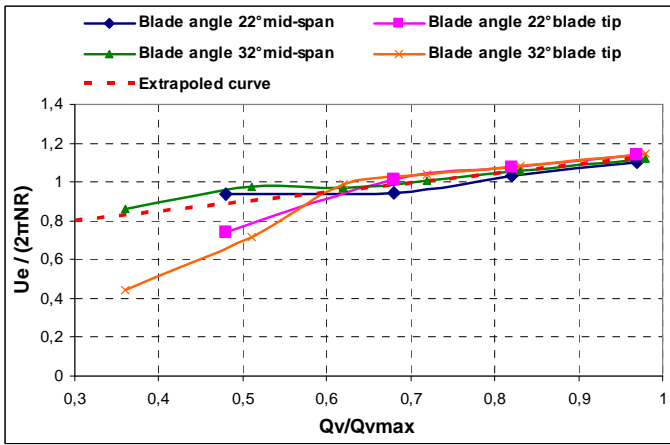


Fig. 21 Evolution of U_e with flowrate (the red dotted line is obtained from an extrapolation of the calculated data at high flowrate)

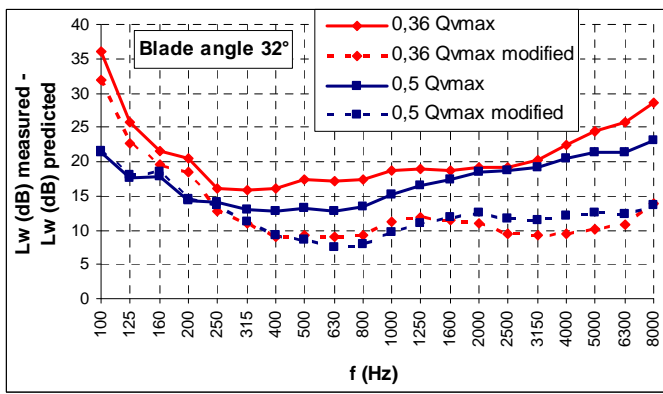
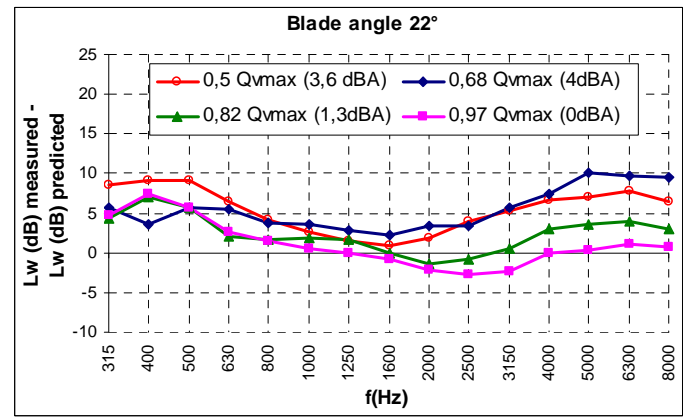


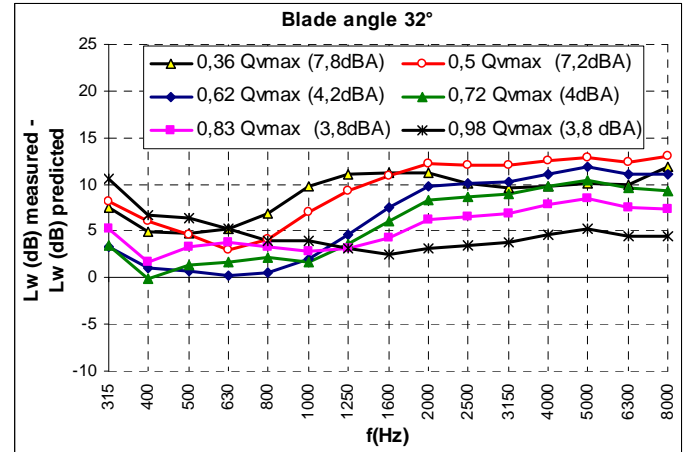
Fig. 22 Influence of δ^* and U_e on the prediction $\beta_0=32^\circ$ (continuous lines: initial prediction; dotted lines: prediction after modifications shown in Fig. 20 and Fig. 21)

Influence of the tip vortex noise. A test was made to try to reduce the contribution of the tip vortex noise on the measured fan sound power spectra. A tip vortex control device looking like that shown in [13] was taped to the pressure side of each blade close to the tip. This device allowed to reduce the sound level of about 3 dB in a large frequency range for $\beta_0 = 22^\circ$ but the noise reduction was negligible for $\beta_0 = 32^\circ$. It was out of the scope of this work to start an extensive research to reduce the tip vortex noise on this fan. This limited test proved this additional source might partly explain the underestimation of the prediction.

Final results. Fig. 23 presents the difference $\Delta L_W(f)$ in the frequency range [315 Hz – 8kHz] for $\beta_0 = 22^\circ$ and 32° and different operating points after applying the various modifications proposed above to improve the prediction. The difference in the A-weighted overall sound power levels between the experiment and the prediction is also pointed out in the figure. These results clearly confirm that the prediction is the closest to the experiment at high flowrate when $\beta_0 = 22^\circ$.



(a)



(b)

Fig. 23 Difference in levels between the measured and predicted spectra after improvements in the prediction (a) $\beta_0 = 22^\circ$; (b) $\beta_0 = 32^\circ$

DISCUSSION AND CONCLUDING REMARKS

The objective of this study was to attempt to validate a semi-empirical method to predict the blade trailing-edge noise of an axial-flow fan non-equipped with embedded pressure transducers. The proposed method rests on a prediction model which uses input data deduced from non-dimensional spectra and correlation lengths of the blade pressure fluctuations obtained in previous studies and RANS simulations. The agreement between the predicted and measured fan sound power spectra may appear disappointing but several reasons can explain the discrepancies between predicted and test results, which are sum up below. Let us recall first that a prediction model aims to provide reliable results in terms of relative levels. It may be considered as satisfactory if it gives right trends when parameters such as fan geometry, blade angle, operating point are varied.

The prediction model itself does not seem to be the cause of the disagreement, except in the frequency range below 315 Hz, since it has been successfully validated on various

stationary airfoils in wind tunnels and the adjustments made to account for the blade rotation do not appear problematic.

The main reasons of the discrepancies between the measured and predicted sound levels are most likely due to the contribution of additional source(s) not taken into account in the prediction, such as tip vortex noise, and the inaccuracy of the input data of the model.

Unlike the tests on a single airfoil in wind tunnel, the actual contribution of the different broadband noise sources of an axial fan cannot be clearly assessed because of the complexity of the 3D flow pattern on the blades. In the present study the fact that the prediction systematically underestimates the level could partly be due to the presence of one or several additional sources. The attempt made here to reduce the amplitude of the tip vortex noise with some rudimentary winglets on the tip was not successful for $\beta_0 = 32^\circ$. Further work to assess the contribution of the tip vortex noise to the total noise radiated by the fan whatever the blade angle and the operating point would be highly beneficial. Questions are raised on the origin of the tip vortex noise itself. Is it due to the interaction of the vortex with the tip edge or with the trailing edge? May it also be due to the impingement of the vortex issued from one blade on the adjacent blade? RANS simulations show that the detachment of the vortex from the blade tip occurs closer to the leading edge when the flowrate is reduced. It may be anticipated that the potential interaction of the tip vortex with an adjacent blade could likely occur at low flow more than at high flow rate.

As already mentioned above a noise source due to the interaction of the inlet turbulent flow with the blades is most unlikely in the present study since the noise level would increase with the flow rate. That would contradict the fact that the prediction is always closer to the experiment at high flow rate.

The inaccuracy of the dimensional input data of the model, especially the inaccuracy of the wall-pressure spectra along the blade span, may be another cause of disagreement between experiment and prediction. In the four-blade axial fan mentioned in the paper the input data were measured at two radial locations only, at mid-span and close to the tip, even if the span was split up into six segments in the prediction. It was assumed that the statistics of the pressure fluctuations at these two spanwise positions were representative of what happened along the whole span, which may be questionable. Furthermore, the possible influence of the tip vortex on the wall-pressure statistics measured with the sensors close to the blade tip could not be assessed.

Finally, the inaccuracy of the generic non-dimensional spectrum and spanwise correlation length of the blade pressure fluctuations on the six-blade fan may also be a source of discrepancies. Indeed, the shape and amplitude of the non-dimensional wall-pressure spectrum near the trailing edge of an airfoil strongly depends on the chordwise mean pressure gradient and the history of the boundary layer convected from the leading edge [9]. The choice of a generic non-dimensional spectrum representative of quite different flow conditions and blade shapes may appear arbitrary. Furthermore, the choice of

the outer variables δ^* and U_e to normalize the spectrum may be debatable since the outer variables are representative of the low frequency part of the wall-pressure spectrum, while the inner variables (wall shear stress, kinematic viscosity and friction velocity) account for the higher frequency. However, the numerical estimation of the inner variables requires a very fine meshing of the blade boundary layer, which implies a large computation time for a non-guaranteed result. Further experimental and numerical works would be most valuable to enlarge the database of non-dimensional wall-pressure spectra on axial fans for different blade shapes and operating conditions.

ACKNOWLEDGMENT

The authors kindly acknowledge the sound comments of the reviewers that allowed clarifying some points and hopefully contributed to improve the quality of the initial draft.

REFERENCES

- [1] Amiet, R.K., 1976, "Noise due to turbulent flow past a trailing edge," *J. Sound Vib.*, 47(3), pp. 387-393.
- [2] Brooks, T. F. and Hodgson, T.H., 1981, "Trailing edge noise prediction from measured surface pressures," *J. Sound Vib.*, 78(1), pp. 69-177.
- [3] Moreau, S. and Roger, M., 2009, "Back-scattering correction and further extensions of Amiet's trailing-edge noise model. Part 2: Application," *J. Sound Vib.*, 323, pp. 397-425.
- [4] Roger, M. and Moreau, S., 2005, "Back-scattering correction and further extensions of Amiet's trailing-edge noise model. Part 1: Theory," *J. Sound Vib.*, 286(3), pp. 477-506.
- [5] Roger, M., Moreau, S. and Guédél, A., 2006, "Broadband fan noise prediction using single-airfoil theory," *Noise Control Eng. J.*, 54(1), pp. 5-14.
- [6] Roger, M. and Moreau, S., 2010, "Extensions and limitations of analytical airfoil broadband noise models," *Aeroacoustics* 9(3), pp. 273-305.
- [7] Schlinker, R.H. and Amiet, R.K., 1981, "Helicopter rotor trailing edge," *Tech. Rep. CR - 3470*, NASA.
- [8] Guédél, A., Rozenberg, Y., Roger, M. and Perrin, G., 2009, "Experimental validation of a model of fan trailing-edge noise," *Noise Control Eng. J.* 57(4), pp. 318-326.
- [9] Rozenberg, Y., Moreau, S., Henner, M. and Morris, S.C., 2010, "Fan trailing-edge noise prediction using RANS simulations," *AIAA Paper* pp. 2010-3720.
- [10] Carolus T., Schneider M., Reese H., 2007, "Axial flow fan broad-band noise and prediction", *J. Sound Vib.*, 300, pp. 50-70
- [11] Howe, M.S., 1978, "A review of the theory of trailing-edge noise", *J. Sound Vib.*, 61(3), pp. 437-465
- [12] Rozenberg, Y., Roger, M. and Moreau, S., 2010, "Rotating blade trailing-edge noise: experimental validation of analytical model," *AIAA J.*, 48(5), pp. 951-962.
- [13] Longet, C. and Battistoni, F., 2003, "Design of a low noise axial fan," *Proc. Fan Noise Conference*, Senlis, France.